IEEE Access
Multidisciplinary ⋮ Rapid Review ⋮ Open Access Journal

Received February 14, 2022, accepted April 13, 2022, date of publication April 29, 2022, date of current version May 11, 2022.

Digital Object Identifier 10.1109/ACCESS.2022.3171231

Optimization of All-Textile Capacitive Sensor Array for Smart Chair

HELENA GLESKOVA[1], (Senior Member, IEEE), AMAYIKAI A. ISHAKU[1], TADEÁŠ BEDNÁR[2,3], AND RÓBERT HUDEC[4]

[1]Department of Electronic and Electrical Engineering, University of Strathclyde, Glasgow G1 1XW, U.K.
[2]Department of Theoretical Electrical Engineering and Biomedical Engineering, University of Žilina, 010 26 Žilina, Slovakia
[3]Scheidt & Bachmann Slovensko, 012 32 Žilina, Slovakia
[4]Department of Multimedia and Information-Communication Technology, University of Žilina, 010 26 Žilina, Slovakia

Corresponding authors: Helena Gleskova (helena.gleskova@strath.ac.uk) and Róbert Hudec (robert.hudec@feit.uniza.sk)

This work was supported by the European Union's Horizon 2020 Research and Innovation Program under the Marie Skłodowska-Curie under Grant 734331.

ABSTRACT All-textile capacitive sensor arrays made of a polyurethane foam, fabric and electrically-conducting yarn were fabricated for a 'smart chair'. Polyurethane foam slab that functioned as a dielectric medium was encased between two pieces of commercially available fabric. The electrically-conducting yarn was used to embroider the capacitor electrodes on both fabric pieces. The completed sensor arrays were investigated under normal compressive load with the targeted pressure range of 2 to 30 kPa for the chair seat and 2 to 8 kPa for the backrest. The sensor capacitance versus normal compressive load exhibited a load/unload hysteresis for all sensor arrays. The hysteresis was modelled with sigmoid function and much narrower hysteresis was observed when all sensors were loaded simultaneously, as opposed to their individual loading, allowing development of a phenomenological model for the former. Among the studied sensor arrays, the array with dimensions of 30 cm × 30 cm made of a 10-mm-thick polyurethane foam with density of ∼18.6 kg/m^3 was the most suitable for the following reasons: (a) unloaded sensor capacitance was ∼2.7 pF, (b) the sensor location did not affect its response, (c) ∼10 kg load applied across individual sensor raised its capacitance by ∼12 pF, and (d) 60 kg load applied uniformly across the whole sensor array increased the capacitance by ∼5 pF. During the compression of the individual sensors the top fabric affected the sensor's electro-mechanical response and elastic fabric would be favored for applications with non-uniform pressure distribution.

INDEX TERMS Capacitive sensors, polymer foams, sensor arrays, smart devices, textiles.

I. INTRODUCTION

The mass-penetration of computers and smart devices in workplaces and homes has caused a gradual shift from active to sedentary lifestyles. Much time is spent sitting while working/learning, commuting, or lounging and reduction in physical activities is becoming the norm. Studies of the recent Covid-19 pandemic have shown a significant growth in sedentary lifestyles, particularly among teens and young adults, caused by the lockdown restrictions [1]. Poor sitting habits are on the rise, causing musculoskeletal disorder (MSD) accompanied by muscular and joint pain [2]. MSD is accountable for most of the work-related health problems often resulting in two-to-six week leave of absence [3] and costing billions in annual compensation [4]. In 2013/2014, the UK reported 8.3 million days of lost work averaging ∼15 days for each case of MSD; Germany reported 95 million days, and 34% of all lost workdays were due to MSD in USA [4].

Various approaches were proposed for reducing the risk of MSD through detection of poor sitting postures or real-time intelligent monitoring of sedentary behaviors, including vision camera tracking real-time postures [5], [6] and wearable inertia sensors (accelerometers) attached to the body or spine [7], [8]. But perhaps the most popular solutions use smart textile sensors integrated into garments [9]–[12] and 'smart' or 'intelligent' chairs or seat platforms embedded with commercial flexible sensors [13]. However, to date much of the research has focused on machine learning algorithms and internet of things (IoT) solutions and less on the electro-mechanical aspects of the sensor cushion.

Among various solutions proposed to date, the integration of novel textile sensors in an all-textile smart chair would be the most desirable for the following reasons: (a) tex-

The associate editor coordinating the review of this manuscript and approving it for publication was Xiaokang Yin.

tile sensors are inherently compatible with the current chair designs, (b) the placement of the sensors into the chair and not on the user does not invade the user's comfort, and (c) the continuous filming of the user is avoided. We present such an approach based on novel capacitive sensor arrays that use polyurethane foam slabs and commercial fabrics embroidered with electrically-conductive yarns. The advantage of this sensor design is that with the exception of the conductive yarn the remaining materials are typical for the upholstered chairs.

The pressure distribution inflicted by the sitting person compresses the foam that acts as a dielectric medium in the textile capacitor. Polyurethane foams have other benefits, i.e. they have been extensively studied under tension and compression [14], [15] and their mechanical models exist [16]. In addition, polyurethane foams are lightweight, breathable, portable, washable, easily embeddable into any textile platform, and commonly used in soft furnishing. Electrically-conductive yarn is used to embroider the electrode areas on suitable fabrics. It is worth noting that the traditional design of the chair can remain essentially unaltered and the sensor cushion is simply integrated into the seat and backrest padding. However, understanding of the electromechanical response of the all-textile capacitive sensor arrays is needed.

II. EXPERIMENTAL DETAILS

Nine capacitive all-textile sensors arranged in 3 × 3 square pattern (Fig. 1(a)) were investigated for the seat and backrest of a 'smart chair'. The fabrication of the capacitive sensors can be split into three main stages: (i) embroidery design of the sensor electrodes in Wilcom Deco Studio software, (ii) embroidery of the top and bottom electrode arrays using Barudan embroidery machine and electrically-conductive yarns, and (iii) the sensor array assembly. A gabardine fabric[1] with thickness of 0.4 mm was selected for the embroidery of the electrode arrays. A 4 mm × 4 mm star pattern (Fig. 1(c)) was chosen to cover the 40 mm × 40 mm electrode area (Fig. 1(b)) of each capacitive sensor. The star pattern was selected as a compromise between the area coverage and the drapability of the completed electrodes. The gap between the neighboring electrodes was 40 mm in both directions, i.e. the electrodes were arranged on an 80-mm square grid. An electrically-conductive yarn 3ltex[2] with resistance of 140 Ω/m was used to sew the electrodes. The resistance of the embroidered electrodes, measured side to side, was ∼0.5 Ω. The implementation of the star pattern when compared to a 'solid' metal electrode made of Al foil led to ∼15% reduction in the sensor capacitance. The sensors were connected vertically in the top electrode fabric (Fig. 1(a)) and horizontally in the bottom one. The fully-automated sewing of each electrode array included nine electrodes, 'wiring' between the electrodes (Fig. 1(d)), and pads for attaching the press fasteners to enable the connection of the measurement equipment to the rows and columns of the sensor array. The press fasteners can be seen in Fig. 1(a).

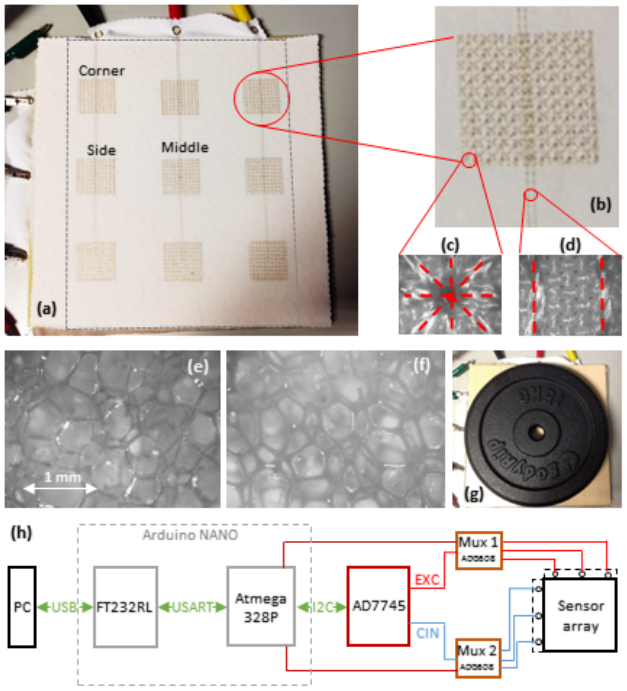

FIGURE 1. Top view of the ∼30 cm × ∼30 cm × 1 cm sensor array (Type 1 polyurethane foam) with 3 × 3 textile electrodes on top (visible, connected vertically) and bottom (hidden, connected horizontally) (a); top view of a 4 cm × 4 cm textile electrode made of 10 × 10 star patterns (b); a single star pattern embroidered using electrically-conducting yarn (c); parallel conducting lines connecting individual textile capacitors (d); micro-structure of polyurethane foam Type 1 (e) and Type 2 (f); sensor array of (a) loaded with 15 kg (g), and block diagram of the simultaneous measurement of the whole sensor array (h). The dashed rectangle in (a) shows the size of the Type 2 sensor array. Corner, Side and Middle denote the position of the individual sensors within the sensor array.

To complete the capacitive sensor array the fabric with bottom electrodes, polyurethane foam slab of a certain thickness, and the fabric with the top electrodes were aligned and assembled into a single unit. The process involved placing a hot-melt adhesive film between the individual layers and applying temperature of 120 °C for 15 s in a heat press. Two types of polyurethane foams were used and are referred to as Type 1 (Fig. 1(e)) and Type 2 (Fig. 1(f)). Type 1 and Type 2 had density of 18.63 ± 0.13 and 27.90 ± 0.29 kg/m^3, respectively. For Type 1 thicknesses of 10 mm and ∼38 mm were selected, whereas Type 2 was either ∼13 mm or 38 mm thick, leading to 4 different sensor arrays. In addition, the completed Type 1 sensor arrays were square with horizontal dimensions of ∼30 cm × ∼30 cm (Fig. 1(a)), whereas the completed Type 2 sensor arrays were rectangular with horizontal dimensions of ∼22 cm × ∼30 cm (blue dashed rectangle in Fig. 1(a)). Consequently, the sensors within Type 1 sensor array were distanced from the edges, while

[1]Gabardine is a tightly woven fabric made with a twill weave. It is a relatively strong and firm cloth. Several varieties exist, the one used here is 100% polyester.

[2]3ltex is woven from electrically-conductive fibers with antioxidant treatment. The treatment protects the electrically-conductive surface coating of the individual fibers, making the fibers and the whole yarn durable. 3ltex was selected from a variety of yarns and supplied by the Research Institute of Textile Chemistry CHEMITEX, Žilina, Slovakia.

some sensors in Type 2 array were close to an edge. Fig. 1(a) also denotes the naming of the individual sensors within the sensor arrays as Corner, Side and Middle.

Two types of compressive loading experiments were performed. During the first one, the sensors were loaded individually and their capacitance was measured between the corresponding row and column lines using Agilent B1500A parameter analyzer equipped with a capacitance module. A thick, circular glass disk with a diameter of 6.2 mm was placed on the top electrode of a particular sensor and the load was applied in the normal direction. The sensor depression was measured with a precision micrometric screw. Loads of up to ∼18 kg were used, allowing compressive strain from 0 to ∼80%.

The second loading experiment involved the simultaneous measurement of the dynamic change in capacitance of the whole sensor array, with all sensors loaded uniformly (see Fig. 1(g)). A 24-bit, 1-channel, high-resolution capacitance-to-digital converter (AD7745) was used for the measurement of the sensor capacitance. Input range of AD7745 is ∼8.2 pF, while it can accept up to 17 pF of common-mode capacitance, set up by the programmable on-chip registers. The block scheme of the whole system is depicted in Fig. 1(h). Arduino NANO was used for the communication between AD7745 and a personal computer. Since the chip has only one channel, an auxiliary circuit, allowing the measurement of multiple sensors, was used. This circuit was composed of two multiplexors; the first one for routing the excitation signal and the second one for routing the measured signal. During the measurement the columns were sequentially excited and the row capacitances were measured, allowing a separate measurement of each sensor. A comparable system is presented in [17]. Since the sampling rate of AD7745 was 90.9 Hz, the capacitance of each sensor was measured approximately 10 times per second. The firmware for ATMEGA328P was created in Atmel Studio and MATLAB® was used to store and graph the data on the PC.

III. EXPERIMENTAL RESULTS

Fig. 2 summarizes the measurements obtained on the two thinner fabric sensor arrays containing polyurethane foam of Type 1 (Fig. 2(a), 2(b), 2(c), 2(d)) and Type 2 (Fig. 2(e), 2(f), 2(g), 2(h)). Each sensor was loaded individually and its response with respect to its position within the sensor array was monitored. Fig. 2(a) and 2(e) show the sensor thickness as a function of the compressive load for Middle, Side, and Corner sensors, while Fig. 2(b) and 2(f) depict the sensor capacitance as a function of the load. The conversion of the load (in kg) to pressure/stress (in kPa) is also given. A reduction in the sensor thickness and an increase in the sensor capacitance were observed with increasing compressive load, for both sensor arrays. The response was nonlinear, i.e. a region of a slow change was followed by a region of faster change and then followed by another region of a slower change. For Type 1, the initial sensor capacitance was ∼2.6 pF (unloaded) and the capacitance for the maximum

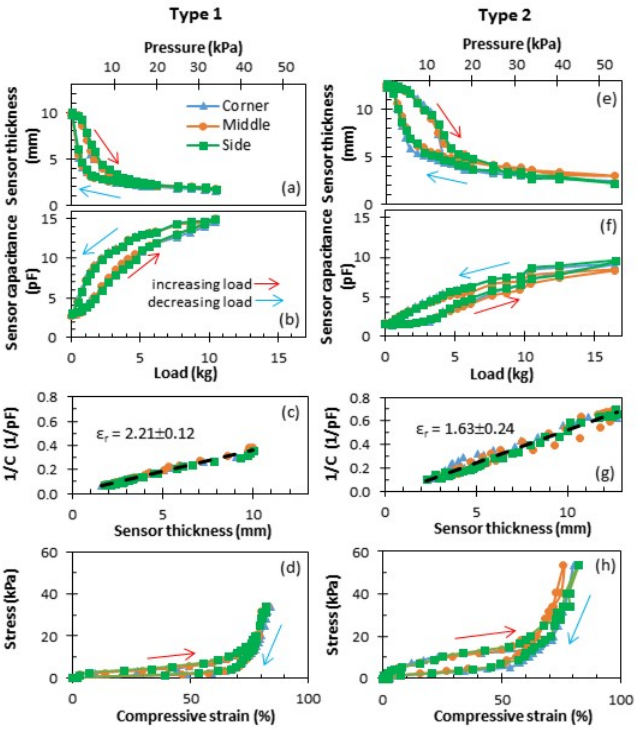

FIGURE 2. Sensor thickness (a, e) and sensor capacitance (b, f) as functions of compressive normal load; inverse sensor capacitance versus sensor thickness (c, g); and stress-strain curves (d, h) for sensors in different locations of the sensor array, for polyurethane foam Type 1 (a, b, c, d) and Type 2 (e, f, g, h). Both the load (kg) and pressure/stress (kPa) are shown in (a), (b), (e), and (f).

load of ∼10.5 kg reached ∼15 pF. For Type 2, the initial sensor capacitance was ∼1.5 pF (unloaded) and the capacitance for the maximum load of ∼16.5 kg reached ∼9 pF. The reduction of the load back to 0 led to an increase in the sensor thickness and the decrease in the sensor capacitance; however, hysteresis for the load/unload cycle was observed.

For Type 1, the response is similar regardless of the location of the sensor within the array, whereas for Type 2 the Middle sensor has slightly weaker response when compared to the Side and Corner sensors. This results from the competing mechanical forces that exist during the compression of the individual sensors. Namely, the normal compressive force is countered by the in-plane tensile forces that develop in the top fabric around the compressed sensor.

Fig. 2(c) and 2(g) show the reciprocal of the sensor capacitance plotted as a function of the sensor thickness. A linear relationship is observed for both polyurethane foams, leading to relative permittivity of 2.21 ± 0.12 for Type 1 and 1.63 ± 0.24 for Type 2. Finally, Fig. 2(d) and 2(h) show the stress-strain hysteresis obtained during the load/unload cycle. This is anticipated because polyurethane foams exhibit load/unload hysteresis. While both sensor arrays were subjected to compressive strain of up to ∼80%, Type 2 required about 50% larger compressive stress to achieve that, when compared to Type 1. At the same time, Type 2 exhibited

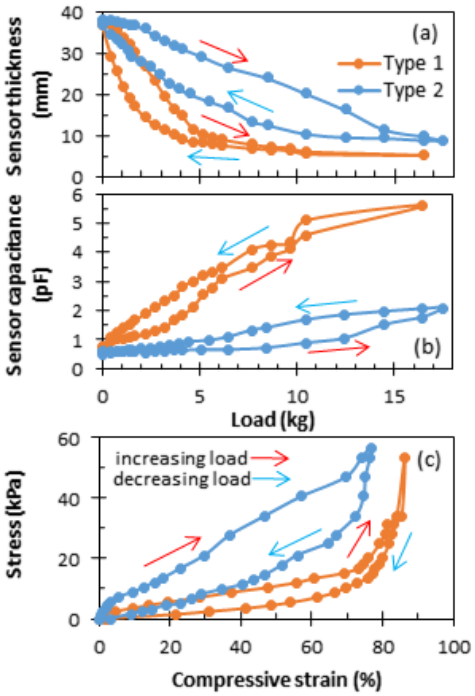

FIGURE 3. Sensor thickness (a) and sensor capacitance (b) as functions of compressive normal load; and stress-strain curves (c) for individually-compressed capacitive sensor in Type 1 and Type 2 sensor arrays. The conversion between load (kg) and pressure/stress (kPa) is shown in Figure 2.

smaller change in the sensor capacitance when compared to Type 1.

Fig. 3 shows a comparison between Type 1 and 2 sensor arrays when ∼38-mm-thick polyurethane foam is used. Again, a response from an individually compressed capacitive sensor is shown. Fig. 3(a) shows the change in the sensor thickness as a function of compressive load, Fig. 3(b) shows the change in the sensor capacitance with load, and Fig. 3(c) depicts the stress-strain curves. The maximum load of ∼17 kg leads to the capacitance of 5.6 pF at the sensor thickness of 5.2 mm for Type 1 and the capacitance of 2.1 pF at the sensor thickness of 8.9 mm for Type 2. That corresponds to stress of ∼54 kPa at the compressive strain of ∼86% for Type 1 and ∼57 kPa at the strain of ∼77% for Type 2. The unloaded sensor capacitance was ∼0.8 and ∼0.6 pF for Type 1 and Type 2, respectively.

Next, normal compressive load was applied uniformly to the whole sensor array and all 9 sensors were measured simultaneously. Load/unload hysteresis was measured for loads up to 30, 40, 50 and 60 kg, leading to the maximum normal pressure/stress of 3.27, 4.36, 5.45, and 6.54 kPa, respectively. Fig. 4 depicts the change in capacitance for all 9 sensors as a function of pressure for the thin Type 1 sensor array. All sensors have similar response, although small variations exist that are not correlated with the sensor location. Initially, there is little change in the sensor capacitance with increasing pressure of up to ∼2 kPa, followed by a distinctive rise in

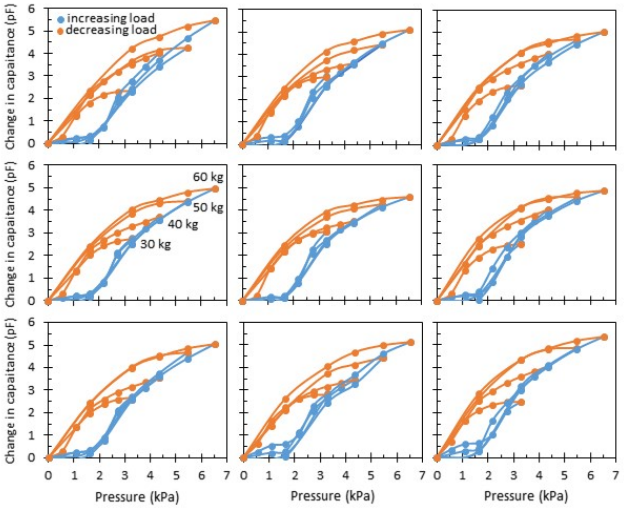

FIGURE 4. Change in sensor capacitance as a function of normal compressive pressure. Simultaneous measurement from all 9 sensors is shown.

capacitance for higher pressure. The maximum load of 60 kg led to an overall increase in the sensor capacitance of ∼5 pF. When the same experiment was performed on the thicker Type 1 sensor array, the maximum load of 60 kg led to an overall increase in the sensor capacitance of ∼1.5 pF.

Compared to the individually compressed sensors a reduced load is required to achieve the same compressive strain when the whole sensor array is loaded evenly. That is because the normal compressive load applied uniformly to the whole array is transformed into compressive strain without a need to counter in-plane tensile forces developed within the sensor array, e.g. in the top fabric.

IV. DISCUSSION

The pressure distribution while sitting in an office chair was shown to depend on the geometry and material properties of the chair [18]. In addition, the anatomy of the seated buttocks on polyurethane foam was shown to vary from person to person depending on the ischial tuberosity's bone structure, muscle tissue deformation, and subcutaneous fat around the glutes, thus affecting the pressure/stress distribution [19]. The pressure peaked in the locations of ischial tuberosities and decreased gradually in all directions [20]. The pressure under the ischial tuberosities was 1-3 N/cm^2 (10-30 kPa), followed by 0.8-1.5 N/cm^2 (8-15 kPa) in the area around the tuberosities, and 0.2-0.8 N/cm^2 (2-8 kPa) in the remaining areas of the seated buttock and backrest [21]. Consequently, the all-textile sensor cushion should be capable of monitoring pressure/stress from 2 to 30 kPa.

Based on Fig. 2 both types of thinner polyurethane foam can accommodate the compressive pressure/stress exhibited by a seated person. For Type 1 the stress between 0 and 30 kPa required compressive strains between 0 and 80%. The location of the sensor did not play a role and the absolute change in the sensor capacitance was larger than for Type 2.

The slightly thicker Type 2 led to a larger range of compressive stress (up to ca 50 kPa), but somewhat reduced change in the sensor capacitance (ca 35%).

For the thicker polyurethane foams, Type 1 exhibited larger change in capacitance and larger strain for similar loads. In addition, having similar unloaded sensor thicknesses, Type 1 displayed smaller hysteresis, making it more suitable for practical sensor development. Consequently, the Type 1 sensor arrays seem more suitable for incorporation into the smart chair.

While the polyurethane foams readily respond to locally applied compressive loads, polyurethane foams covered with fabric with high tensile strength behave differently. In our case the top fabric does not provide the in-plane elasticity needed to accommodate the mechanical deformation around the compressed sensor and works against the normal compressive force. Consequently, the same normal compressive load applied locally led to a slightly larger reduction in the sensor thickness if the sensor was located near the edge of the sensor array. However, when the distance of the sensor from the edge was ∼40 mm, the position of the sensor within the sensor array did not matter and all sensors responded in a similar manner.

The results were somewhat different when the compressive load was applied uniformly across the whole sensor array. In such a case the top fabric is not under tension and its tensile strength does not work against the applied normal load. Consequently, the capacitors are compressed more easily, i.e. about half of the compressive pressure/stress is needed to achieve strain comparable to that of the individually loaded sensors. However, when a person would sit on the sensor array embedded in a smart chair, the non-uniform distribution of the pressure would generate in-plane tensile forces within the top fabric and the maximum sensed pressure is estimated to be between ∼10 and ∼30 kPa for the thinner Type 1 sensor array. Therefore, the sensor array would be able to measure the pressure of the leaning back and the 'softer' areas of the seated buttock and it is likely to reach saturation under the ischial tuberosities.

Next, we compared the hysteresis of the load/unload cycle of Fig. 2 and 4. To do that, sigmoid functions [22] were used to model the load/unload hysteresis. Fig. 5(a) shows the change in capacitance of the uniformly loaded sensor array based on the thinner Type 1 foam. The points represent the measured change in the sensor capacitance ΔC averaged across all 9 sensors (refer to Fig. 4), with the corresponding standard deviations, and the lines are the sigmoid least-square fits to the data. The load part of the hysteresis is modelled as:

$$\Delta C = \frac{A_1 exp\left[A_2\left(\sigma + A_3\right)\right]}{A_4 + exp\left[A_5\left(\sigma + A_3\right)\right]} + A_6\left(\sigma + A_3\right) \qquad (1)$$

where σ is the applied normal compressive stress in kPa, ΔC is in pF, and A_1, A_2, A_3, A_4, A_5, and A_6 are constants, namely, $A_1 = 2.5061$, $A_2 = 2.2246$, $A_3 = -0.94705$, $A_4 = 25.574$, $A_5 = 2.1$, and $A_6 = -5.2779 \times 10^{-3}$. The unload part of the hysteresis depends on 'the point of return' and the capacitance at the return point is denoted as ΔC_R. While (1) is still used to model the unload behavior, A_1, A_2, A_3, A_4, and A_5 are functions of ΔC_R, namely

$$\begin{aligned} A_1 &= \Delta C_R \\ A_2 &= -1.6629 + \frac{11.815}{\Delta C_R} \\ A_3 &= -0.0079307 \cdot exp\left(1.1644 \cdot \Delta C_R\right) \\ A_4 &= 4207.9 \cdot exp\left(-1.842 \cdot \Delta C_R\right) \\ A_5 &= -1.803 + \frac{13.26}{\Delta C_R} \\ A_6 &= 0.6 \end{aligned} \qquad (2)$$

Four different ΔC_R values corresponding to the maximum loads of 30, 40, 50, and 60 kg result in four unload curves that reproduce the sensor measurements (see Fig. 5(a)). While the above model is phenomenological, it allows to calculate the change in sensor capacitance as a function of applied compressive stress while taking into account the load/unload hysteresis.

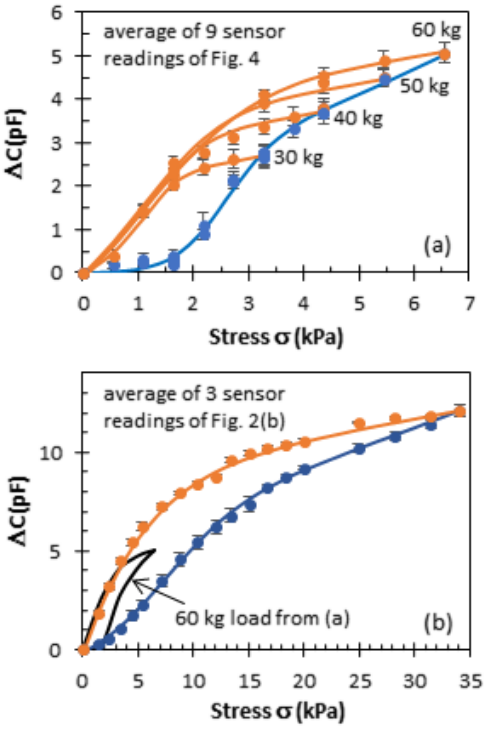

FIGURE 5. Change in sensor capacitance as a function of normal compressive stress for the concurrent (a) and individual (b) loading of the sensors. The points represent the measured average capacitance values and the lines are sigmoid fits based on (1).

Fig. 5(b) shows the change in capacitance versus the normal compressive stress, for the individually compressed sensors. The points represent the measured change in the sensor capacitance ΔC averaged across 3 sensors (refer to Fig. 2(b)), with the corresponding standard deviations, and the lines are the sigmoid least-square fits to the data. Equation (1) was used to fit both the load and unload parts of the hysteresis.

A comparisons to the uniformly compressed sensor array is also provided. When the sensors are compressed individually, the load/unload hysteresis is visibly widened and stretched in the horizontal direction, result of the rigidity of the top sensor fabric. This horizontal elongation of the load/unload hysteresis is manifested by about an order of magnitude lower values for A_2 and A_5. Consequently, top fabric with higher in-plane elasticity would reduce the load/unload hysteresis and simplify the interpretation of the sensor response.

Finally, local application of normal compressive stress to the sensor array leads to tensile strain in the top fabric, especially around the compressed area. This strain can be reduced by using a thinner polyurethane slab in the sensor array. Large tension may affect the electrical integrity of the array and the connections between the sensors are the most vulnerable.

REFERENCES

[1] C. Zheng, W. Y. Huang, S. Sheridan, C. H. P. Sit, X. K. Chen, and S. H. S. Wong, "COVID-19 pandemic brings a sedentary lifestyle in young adults: A cross-sectional and longitudinal study," *Int. J. Environ. Res. Public Health*, vol. 17, no. 17, p. 6035, Sep. 2020, doi: 10.3390/ijerph17176035.

[2] J. H. Park, J. H. Moon, H. J. Kim, M. H. Kong, and Y. H. Oh, "Sedentary lifestyle: Overview of updated evidence of potential health risks," *Korean J. Family Med.*, vol. 41, no. 6, pp. 365–373, Nov. 2020, doi: 10.4082/KJFM.20.0165.

[3] F. Lötters and A. Burdorf, "Prognostic factors for duration of sickness absence due to musculoskeletal disorders," *Clin. J. Pain*, vol. 22, no. 2, pp. 212–221, 2006, doi: 10.1097/01.ajp.0000154047.30155.72.

[4] O. Korhan and A. A. Memon, "Introductory chapter: Work-related musculoskeletal disorders," in *Work-Related Musculoskeletal Disorders*, Ed. O. Kohran, Ed. Rijeka, Croatia: IntechOpen, Oct. 2019, doi: 10.5772/intechopen.78458.

[5] M. E. A. Elforaici, I. Chaaraoui, W. Bouachir, Y. Ouakrim, and N. Mezghani, "Posture recognition using an RGB-D camera: Exploring 3D body modeling and deep learning approaches," in *Proc. IEEE Life Sci. Conf. (LSC)*, Oct. 2018, pp. 69–72, doi: 10.1109/LSC.2018.8572079.

[6] G. Diraco, A. Leone, and P. Siciliano, "An active vision system for fall detection and posture recognition in elderly healthcare," in *Proc. Design, Autom. Test Eur. Conf. Exhib. (DATE)*, Mar. 2010, pp. 1536–1541, doi: 10.1109/DATE.2010.5457055.

[7] Q. Wang, W. Chen, A. A. A. Timmermans, C. Karachristos, J. B. Martens, and P. Markopoulos, "Smart rehabilitation garment for posture monitoring," in *Proc. 37th Annu. Int. Conf. IEEE Eng. Med. Biol. Soc. (EMBC)*, Aug. 2015, pp. 5736–5739, doi: 10.1109/EMBC.2015.7319695.

[8] M. Gopinath and A. Kirubha, "Real time monitoring of posture to improve ergonomics," *J. Biomed. Eng. Med. Imag.*, vol. 2, no. 2, pp. 22–25, Apr. 2015, doi: 10.14738/jbemi.22.1160.

[9] W. Xu, Z. Li, M.-C. Huang, N. Amini, and M. Sarrafzadeh, "ECushion: An eTextile device for sitting posture monitoring," in *Proc. Int. Conf. Body Sensor Netw.*, May 2011, pp. 194–199, doi: 10.1109/BSN.2011.24.

[10] C. Mattmann, O. Amft, H. Harms, G. Troster, and F. Clemens, "Recognizing upper body postures using textile strain sensors," in *Proc. 11th IEEE Int. Symp. Wearable Comput.*, Oct. 2007, pp. 29–36, doi: 10.1109/ISWC.2007.4373773.

[11] Q. Wang, M. Toeters, W. Chen, A. Timmermans, and P. Markopoulos, "Zishi: A smart garment for posture monitoring," in *Proc. CHI Conf. Extended Abstr. Hum. Factors Comput. Syst.*, May 2016, pp. 3792–3795, doi: 10.1145/2851581.2890262.

[12] A. G. Patiño, M. Khoshnam, and C. Menon, "Wearable device to monitor back movements using an inductive textile sensor," *Sensors*, vol. 20, no. 3, art. 905, pp. 1–17, Feb. 2020, doi: 10.3390/s20030905.

[13] A. A. Ishaku, A. Tranganidas, S. Matúška, R. Hudec, G. McCutcheon, L. Stankovic, and H. Gleskova, "Flexible force sensors embedded in office chair for monitoring of sitting postures," in *Proc. IEEE Int. Conf. Flexible Printable Sensors Syst. (FLEPS)*, Jul. 2019, pp. 1–3, doi: 10.1109/FLEPS.2019.8792250.

[14] W. Witkiewicz and A. Zieliński, "Properties of the polyurethane (PU) light foams," *Adv. Mater. Sci.*, vol. 6, no. 2, pp. 35–51, Oct. 2006. [Online]. Available: http://www.pg.gda.pl/mech/kim/AMS/022006/AMS02200605.pdf

[15] G. L. Oliveira, A. G. Ariza, M. Claire, M. F. Costa, and M. A. Vaz, "Mechanical behavior characterization of polyurethane used in bend stiffener," in *Mechanics of Composite and Multi-Functional Materials*, vol. 7, C. Ralph, M. Silberstein, P. R. Thakre, R. Singh, Eds. Springer, 2016, pp. 99–107.

[16] M. Marvi-Mashhadi, C. S. Lopes, and J. Llorca, "Modelling of the mechanical behavior of polyurethane foams by means of micromechanical characterization and computational homogenization," *Int. J. Solids Struct.*, vol. 146, pp. 154–166, Aug. 2018, doi: 10.1016/j.ijsolstr.2018.03.026.

[17] T. Bednar, S. Borik, and B. Babusiak, "Precise CDC based measurement system for biomedical applications," in *Proc. 12th Int. Conf. Meas.*, May 2019, pp. 123–126, doi: 10.23919/MEASUREMENT47340.2019.8779987.

[18] R. Zemp, W. R. Taylor, and S. Lorenzetti, "Seat pan and backrest pressure distribution while sitting in office chairs," *Appl. Ergonom.*, vol. 53, pp. 1–9, Mar. 2016, doi: 10.1016/j.apergo.2015.08.004.

[19] S. E. Sonenblum, S. H. Sprigle, J. M. Cathcart, and R. J. Winder, "What do we sit on? Anatomy of the seated buttocks," in *Proc. RESNA Annu. Conf.*, 2015. [Online]. Available: https://www.resna.org/sites/default/files/conference/2015/wheelchair_seating/index.html

[20] M. P. Reed. (1994). *Survey of Auto Seat Design Recommendations for Improved Comfort*. [Online]. Available: https://deepblue.lib.umich.edu/bitstream/handle/2027.42/1058/85462.0001.001.pdf

[21] B. Kurz, W. Diebschlag, and F. Heidinger, "Recommendation for ergonomic and climatic physiological vehicle seat design," *J. Cellular Plastics*, vol. 25, no. 2, pp. 125–137, Mar. 1989, doi: 10.1177/0021955X8902500203.

[22] M. Jesenik, M. Mernik, and M. Trlep, "Determination of a hysteresis model parameters with the use of different evolutionary methods for an innovative hysteresis model," *Mathematics*, vol. 8, no. 2, p. 201, Feb. 2020, doi: 10.3390/math8020201.

HELENA GLESKOVA (Senior Member, IEEE) received the B.S. and M.S. degrees in solid state physics, the master's degree in pedagogy and didactics of physics, and the Ph.D. degree in condensed matter physics from Comenius University, Bratislava, Slovakia, in 1985, 1992, and 1993, respectively. From 1993 to 2007, she worked with the Department of Electrical Engineering, Princeton University, Princeton, NJ, USA, where she made seminal contributions to the light-induced metastability in amorphous silicon and was instrumental in the flexible and printable thin-film electronics by developing the first concepts, techniques, and processes for hydrogenated amorphous silicon transistors on plastic substrates. In 2008, she joined the Department of Electronic and Electrical Engineering, University of Strathclyde, Glasgow, U.K., where she established a laboratory for flexible and wearable organic electronics, focusing on low-voltage transistors. She published more than 100 papers and coauthored ten patents. Her current research interests span sensors and sensor systems based on organic materials and novel all-textile approaches.

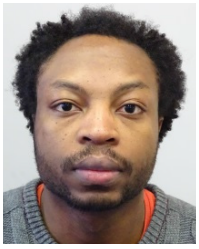

AMAYIKAI A. ISHAKU received the B.Eng. and Ph.D. degrees from the Department of Electronic and Electrical Engineering, University of Strathclyde, Glasgow, U.K., in 2017 and November 2021, respectively. His Ph.D. research focused on the development of sensors and sensor systems for wearable electronics. The sensors exploited low-voltage, high-transconductance organic thin-film transistors and novel all-textile designs. He is currently working with the GKN Automotive Innovation Centre, Abingdon, U.K., where he is involved in the development of state-of-the-art next-generation edrive vehicle technologies within his embedded software and systems roles.

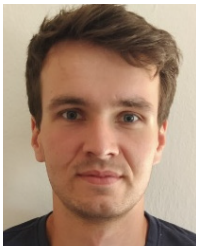

TADEÁŠ BEDNÁR received the M.S. and Ph.D. degrees from the Department of Electromagnetism and Biomedical Engineering, University of Žilina, Slovakia, in June 2018 and August 2021, respectively. His Ph.D. research focused on the analysis and development of textile-based systems for unobtrusive measurement of bioelectrical signals. He is currently working as a Software Developer with Scheidt & Bachmann Slovensko, Slovakia.

RÓBERT HUDEC received the M.S. and Ph.D. degrees from the Faculty of Electrical Engineering and Informatics, Technical University of Košice, in 1998 and 2003, respectively. In 2016, he became a Full Professor with the University of Žilina, Slovakia, where he currently leads the Department of Multimedia and Information-Communication Technology. He published more than 150 papers. He specializes in low-level image feature extraction, 2D/3D image object classification, 3D reconstruction, machine and deep learning, and intelligent health systems, including textile sensors. His research interests include computer vision, bioinformatics, and health applications. He was a recipient of the Werner von Siemens Excellence Award (2003) and Jozef Murgaš Award (2007) for his research on image filtration. In 2006, he received the Prize of the Deputy Prime Minister of Slovakia awarded to the top under-35 researchers in science and technology. In 2017, he and his collaborators from VUTCH-CHEMITEX Žilina, Slovakia, received the Gold Fatima Award for a smart garment prototype that continuously monitors the EKG signals.